Ultrathin acoustic resonating structure based on parallel-arranged Microperforated Panel and deep subwavelength Archimedean-inspired spiral cavities for multi-tonal and broadband sound absorption.

Marco Boccaccio[1], Fabrizio Bucciarelli[1], Gian Piero Malfense Fierro[1],Michele Meo[1],

[1]Department of Mechanical Engineering, University of Bath, Bath, BA2 7AY

Abstract: In recent years, metamaterial-structures and Microperforated panel (MPP) absorbers have been proposed as a valid alternative to porous materials for sound absorption in the low frequency range. However, high and broadband absorption cannot be achieved in the low frequency range as required in some engineering applications where large thicknesses of the absorbers are unsuitable. In this work, a deep subwavelength hybrid parallel-arranged MPP and Archimedean-inspired spiral (AIS) absorber is proposed to obtain broadband sound absorption at low frequency (i.e. 400-2000 Hz). The absorption properties are investigated using an equivalent electro-acoustic model and a parametric analysis is performed to optimise the geometric parameters of the device for the desired frequency range. Two parallel arranged MPPs and AIS structures were designed to achieve sound absorption in frequency ranges between 550-1650 Hz and 380-1250 Hz, with a total thickness less than 1/28 wavelength (24.3 mm). In addition, a parallel arrangement of an AIS and a double layered MPP were also considered to achieve absorption in a wider frequency range (i.e. 480-2800 Hz). The prototypes were then fabricated and tested with an impedance tube to evaluate the normal absorption coefficient via the Transfer Function method (TFM). Experimental results show a good correlation with the analytical models, with a absorption coefficient above 60% over the respective frequency ranges. Moreover, absorption peaks occur at the resonance frequencies and higher harmonics of the structures, with measured values above 95%. The low frequency broadband absorption shown by the proposed subwavelength hybrid structures makes the device suitable for many acoustic engineering applications.

Keywords: Sound Absorption, subwavelength, acoustics, broadband

1. Introduction

In the last decades, researchers have been focused on the development of sound absorbing methods for noise control and cancellation in engineering applications. Conventional materials used for acoustic applications, such as synthetic and porous absorbers[1,2] typically lack absorption properties at low frequencies, since sound attenuation can be expressed as a quadratic function of the frequency. In order to overcome these restraints, both coherent absorbers and vibrating membrane acoustic metamaterials have been proposed to achieve absorption in the low-frequency range [3-5]. However, the absorption properties of these membrane-type systems are limited to a narrow frequency range around the resonance frequencies. Membrane-type metamaterials have been proposed over the year to achieve absorption at low frequencies [6]. These structures exhibit nearly total absorption at resonance frequencies due to flapping motion of asymmetric rigid platelets added to the membranes. However, since the lower frequency limit is imposed by the thickness of the absorbing materials, they become unfeasible in building and constructions applications, where thicknesses, space and weight are highly restrictive. Microperforated panels (MPP) have been proposed as robust fibre-free sound absorbing materials for several applications[7,8]. The basic construction of an MPP system consists of a thin pierced panel placed in front of rigid back wall with an air cavity between them. Consequently, the acoustic performance of MPP structures is determined by the perforation properties (i.e. hole diameter and perforation ratio), the panel thickness and the length of the back cavity. However, MPPs rely on perforation of a few centimetres [9], which results in poorly inherent acoustic resistance and unacceptable absorption in the lower frequency range. Successively, sound absorbing materials have been introduced in the back cavity of an MPP absorber to improve absorption performance at lower frequencies [10]. In particular, a theoretical approach was established to predict sound absorption properties of such a composite structure of sound-absorbing material and MPP. However, introduction of the absorbing materials increases the thickness of the structure, and pollution-free cannot be guaranteed. Maa et al [11-13] further proposed the concept of sub-millimetre perforated panel, which provides sufficient acoustic resistance for high absorption performance and replace fibre materials in circumstances requiring fireproof and restricted environmental conditions, such as acoustic windows systems [14], environmental noise cancelling [15] and duct silencing [16]. In accordance with Maa's theory, the absorption performances of the MPP can be predicted with a maximum error of 6%. Although MPPs have large bandwidth absorption, the absorption properties of these developed structures are strongly dependent on the geometrical

parameters of the system, where low frequency broadband absorption is only achieved with high and unsuitable thicknesses. A combination of MPPs with elastic membranes or honeycomb structures have been successively proposed to obtain broader absorption performance by coupling multiple resonance modes [17-20]. However, additional costs associated with the installation of the honeycomb structure between MPP and rigid back wall play a challenging role in real applications. Parallel-arranged multiple MPPs with different back cavities have been numerically developed furtherly to increase the absorption bandwidth [21]. In this case, the arrangement sequence of three MPP absorber with a total thickness of 98 mm influences the absorption levels between the adjacent resonant peaks. Moreover, a combination of parallel-arranged MPPs with different thicknesses and back cavities and have been developed to broaden the absorption frequency range, compared with single MPP system [22]. The presented prototype can achieve normal incident sound absorption higher than 50% over the frequencies from 370 Hz and 2520 Hz. However, the low-absorption level achieved becomes unsuitable for engineering employment. Successively, a multi-layered MPP prototype has been proposed to achieve broadband absorption over 85% in the frequency range between 400 to 2000 Hz by positioning six plastic perforated panels in series [23]. However, the total thickness of the system (i.e. 132 mm) still represents a challenging problem. The acoustic system for sound absorption proposed in this work addresses both broadening and thickness limitations. The designed structure consists of a parallel arrangement of an Archimedean spiral cavity coiled in plane and perpendicular to the incident wave with monolayered and multi-layered MPP absorbers. We firstly solved the problem of wave propagation in air to derive the acoustic impedance inside a cavity. An analytical model was developed to demonstrate how the acoustic impedance (i.e. the absorption performance) is mainly related to resonance phenomena of the structure. An optimisation process was also performed to relate the geometrical parameters to the acoustic impedance of the system. The optimised prototypes were then designed and fabricated via Stereolithographic 3D printing techniques [24,25], in order to experimentally validate the absorption performance of the hybrid structure. The optimised structure guarantees a broadband absorption above 60% in the low frequency range (i.e. 480-2500 Hz), and high absorption over 95% at the resonant frequencies of the sub-systems with a total thickness of 28.4 mm (i.e. 1/28 wavelength), which results much thinner compared with the structures proposed in the previous works.

2. Theoretical Analysis

2.1. Visco-thermal acoustic theory

Sound propagation in air is associated with small particle displacement velocities, which can be described by second order linear partial differential equations. Assuming propagation of an oscillation in terms of potential wave equation can be written as follows [26,27]:

$$\boldsymbol{\nabla^2\phi = \rho\frac{\partial^2\phi}{\partial t^2}} \tag{2.1}$$

Where $\boldsymbol{\rho}$ is the density of air. For a compressible lossless fluid and small displacement, a potential solution of Eq. (2.1) is given by:

$$\boldsymbol{\phi(x,t) = \frac{A}{\rho\omega^2}e^{j\omega\tau}} \tag{2.2}$$

Where ω is the angular frequency, $\tau = \left(t - x\sqrt{\rho/K}\right)$, K is the bulk modulus of the fluid and A is the amplitude of the propagating sound pressure $p = Aexp(j\tau\omega)$. As a result, assuming unidirectional propagation of the sound pressure (i.e. $r_y = r_z = 0$, $r_x \neq 0$), the displacement vector r can be expressed as:

$$\boldsymbol{r(x,t) = \frac{-jkA}{\rho\omega^2}e^{j\omega\left(t-\frac{x}{c}\right)}} \tag{2.3}$$

with $k = (\omega^2\rho K^{-1})^{1/2}$ being the propagation constant. In the same way, only the x-component of the velocity vector v does not vanish:

$$\boldsymbol{v_x(x,t) = \frac{kA}{\rho\omega}e^{j\omega\left(t-\frac{x}{c}\right)}} \tag{2.4}$$

Eq. (2.3) and Eq. (2.4) can be used to refer to a harmonic plane wave propagating in x-direction. With these regards, pressure and velocities are related by:

$$\boldsymbol{v_x(x,t) = \frac{1}{Z_{ac}}p(x,t)} \tag{2.5}$$

Where the quantity Z_{ac} represents the characteristic impedance of the fluid at the opening of the tube. Assuming plane wave propagating inside a cavity, with length L_t, radius r_{sp} and porosity φ of the system which represents the ratio between the section of the cavity A_t and that of the external environment A_0, the absorption characteristic of the system depends on the acoustic impedance of cavity and that of the air. Acoustic impedance at the opening of the cavity with rigid back wall can be expressed as[26]:

$$\boldsymbol{Z_{sp} = -{}^{Z_{ac}}/_{\varphi}\,cotg(k_{eff}L_t)} \tag{2.6}$$

Where $k_{eff} = \left(\omega^2 \rho_{eff} K_{eff}^{-1}\right)^{1/2}$ is the effective propagation constant, $Z_{ac} = (\rho_{eff} K_{eff})^{1/2}$ is the characteristic impedance of the system, ρ_{eff} and K_{eff} are the effective density and bulk modulus of the air inside the cavity, respectively, and descend from the visco-thermal acoustic theory, as follows [28-30]:

$$\boldsymbol{\rho_{eff}} = \frac{\boldsymbol{\rho_0}}{\mathbf{H(\psi)}} \tag{2.7}$$

$$K_{eff} = -\frac{(\gamma P_0)}{((\gamma - (\gamma - 1)H(\chi/\gamma))} \tag{2.8}$$

Where γ, P_0 and ρ_0 correspond to the specific heat ratio, the air pressure and density, respectively, $\psi = \mu/\rho_0$ is the kinematic viscosity, $\chi = -k_a/\rho_0 C_v$ is the thermal diffusivity, with C_v, μ and k_a denoting the specific heat at a constant volume, air viscosity and thermal conductivity, respectively. The function H(x) of an arbitrary variable x is given by:

$$\mathbf{H(x)} = \mathbf{1} - \mathbf{4}\left(-\frac{\mathbf{j\omega}}{\mathbf{x}}\right)^{-\frac{1}{2}} \mathbf{J_1}\left(\frac{\mathbf{2r_{sp}}\left(-\frac{\mathbf{j\omega}}{\mathbf{x}}\right)^{\frac{1}{2}}}{\mathbf{2}}\right) \Bigg/ \mathbf{J_0}\left(\frac{\mathbf{2r_{sp}}\left(-\frac{\mathbf{j\omega}}{\mathbf{x}}\right)^{\frac{1}{2}}}{\mathbf{2}}\right)\left(\mathbf{2r_{sp}}\right)^{-1} \tag{2.9}$$

Where J_0 and J_1 are the Bessel functions of zeroth and first kind.

2.2. Theory of Microperforated Panel

The MPP consists of a parallel distribution of short cavities with a certain length and separated by a subwavelength distance higher than their diameters. Sound propagation in a hollow duct can be described by considering the equation of aerial motion with the assumption of short tube compared with the incident wavelength [31]:

$$\boldsymbol{\rho_0 \dot{u}} - \frac{\boldsymbol{\eta}}{\mathbf{r_i}} \frac{\boldsymbol{\partial}}{\boldsymbol{\partial r_i}}\left(\mathbf{r_i}\frac{\boldsymbol{\partial u}}{\boldsymbol{\partial r_i}}\right) - \frac{\boldsymbol{\Delta p}}{\mathbf{t_c}} \tag{2.10}$$

Where η is the air viscosity coefficient, r_i represents the radial component of the cylindrical system used to describe the cavity, u is the particle velocity, Δp is the pressure difference applied to back of the cavity, t_c is the length of the cavities and the panel thickness. Eq.(2.10) can be solved for the particle velocity u, in terms of average particle velocity over the cross section of the tube. Therefore, the specific acoustic impedance for a single tube is given by the ratio between the applied pressure difference and the average velocity [32]:

$$\mathbf{Z_i = \frac{\Delta p}{\bar{u}} = j\omega t_c \left[1 - \frac{2}{\delta(-j)^{\frac{1}{2}}} \frac{J_1\delta(-j)^{\frac{1}{2}}}{J_0\delta(-j)^{\frac{1}{2}}}\right]^{-1}} \quad (2.11)$$

Where $\delta = r_0\sqrt{\omega\rho_0/\eta}$ represents the ratio between the inner radius r_0 and the viscous boundary layer thickness inside the tubes, and ranges between 1 and 10 for MPPs[12]. An approximate formula of the opening acoustic impedance of the tube for all δ values is given by [13]:

$$\mathbf{Z_i \cong -\frac{32\eta t_c}{4r_0^2}\sqrt{1+\frac{\delta}{32}} + j\omega\rho_0 t_c\left(1+\frac{1}{\sqrt{9+0.5\delta^2}}\right)} \quad (2.12)$$

Assuming that the holes spacing is larger than the hole diameter, Eq. (2.12) can be extended to the holes of the MPP. Consequently, acoustic impedance of the MPP Z_p will be that of single tube Z_i system divided by the perforation ratio $\boldsymbol{\sigma}$, which represents the ratio between the perforated area and the total area of the panel.

$$\mathbf{Z_P = \left(\frac{Z_i}{\sigma\rho_0 c}\right)^{-1} = \left(\frac{1}{R_i - j\omega X_i}\right)^{-1}} \quad (2.13)$$

$$R_i = -\frac{32\eta t_c}{\sigma\rho_0 c d^2}\sqrt{1+\frac{\delta^2}{32}} + \frac{\sqrt{2}}{8}\delta\frac{d}{t_c} \quad (2.14)$$

$$X_i = -\frac{t_c}{\sigma c}\left(1+\frac{1}{\sqrt{9+0.5\delta^2}} + 0.85\frac{d}{t_c}\right) \quad (2.15)$$

With $d = 2r_0$ being the diameter of the tube. The acoustic impedance is a complex quantity, where the real part (i.e. acoustic resistance) refers to the energy radiation and the viscous losses of the wave propagating within the perforation, whereas the imaginary part represents the mass of the air moving inside the perforation. Furthermore, the MPP system is composed of a single MPP, and a back cavity between the panel and a rigid back wall. With these regards, the acoustic impedance of the air mass in the back cavity can be estimated as follows[26]:

$$\mathbf{Z_D = jc\rho_0\, cotg(Dk)} \quad (2.16)$$

Where D is length of the back-cavity and $k = \omega/c$.

2.3. Acoustic impedance of MPP and series arrangement of MPPs

With the equivalent circuit analogy, the global impedance of the system represents the series between the acoustic impedance of the MPP and that of the back-cavity (Fig 1), and is given by:

$$\mathbf{Z_{MPP} = Z_P + Z_D} \quad (2.17)$$

In the same way, a double-layer MPP systems can be also proposed. In this context, the equivalent system consists of two series-arranged MPP panels with different geometrical properties disposed one by one. Eq. (2.13), Eq. (2.14) and Eq. (2.15) can be still applied to evaluate the acoustic impedance of each MP, Z_{P1} and Z_{P2}. By referring to the equivalent electro-acoustic circuit shown in Fig. 2, the total acoustic impedance is given by:

$$\mathbf{Z_{tot}} = \left(\frac{\mathbf{1}}{\mathbf{Z_{D2} + Z_{p2}}} + \frac{\mathbf{1}}{\mathbf{Z_{D1}}}\right)^{\mathbf{-1}} + \mathbf{Z_{p1}} \tag{2.18}$$

The absorption coefficient α is a function of the acoustic impedance of the system, and is given by:

$$\boldsymbol{\alpha} = \frac{\mathbf{4Re(Z_{tot})}}{\mathbf{[1 + Re(Z_{tot})]^2 + Im(Z_{tot})^2}} \tag{2.19}$$

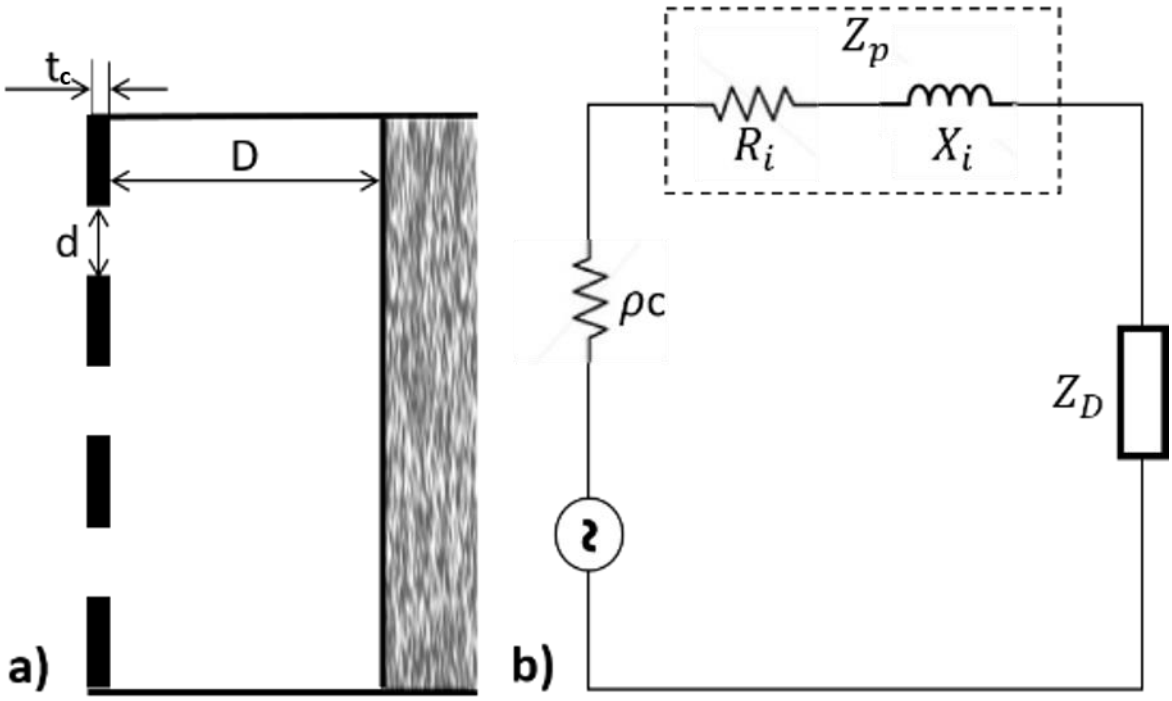

Fig. 1 –a) Microperforated Panel; b) Electro-Acoustical equivalent circuit of an MPP system.

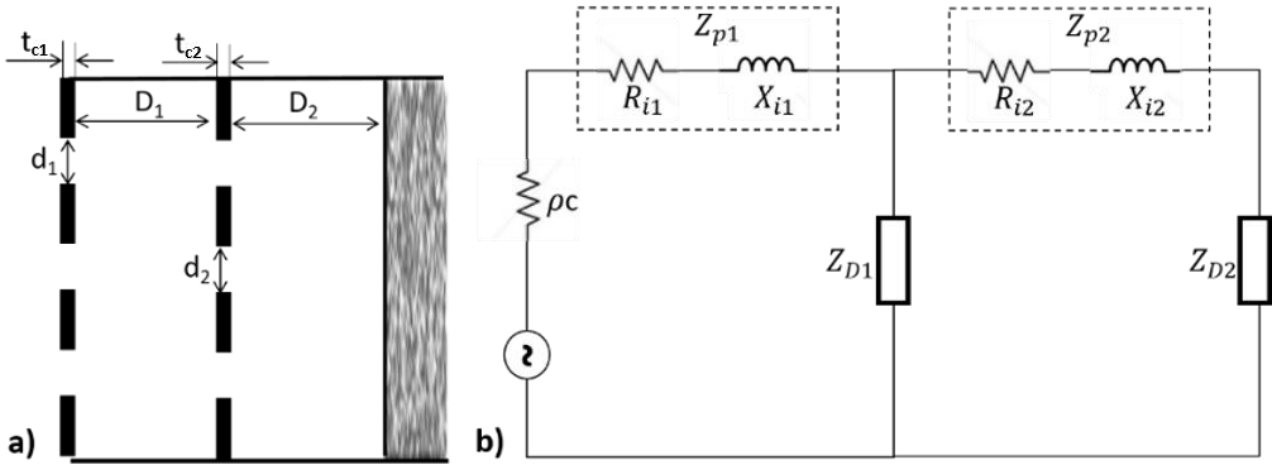

Fig. 2 – a) Double-layer MPP; b) Electro-Acoustical equivalent circuit of double-layer MPP system.

2.4. Acoustic impedance of parallel-arranged MPP and Archimedean-inspired spiral

The parallel-arranged MPP and Archimedean-spiral with the equivalent electro-acoustic circuit model is shown in Fig. 3. According to this, the total acoustic impedance of the system can be evaluated as follows:

$$\mathbf{Z_{tot}} = \left(\frac{\mathbf{1}}{\mathbf{Z_p + Z_D}} + \frac{\mathbf{1}}{\mathbf{Z_{sp} + Z_{c0}}} \right)^{-\mathbf{1}} \tag{2.20}$$

In case of multiple MPPs, the total acoustic impedance can be estimated in accordance with Fig. 4, as:

$$\mathbf{Z_{tot}} = \left(\frac{\mathbf{1}}{\mathbf{Z_{sp} + Z_{c0}}} + \frac{\mathbf{1}}{\mathbf{Z_{d1}}} + \frac{\mathbf{1}}{\mathbf{Z_{D2} + Z_{p2}}} + \mathbf{Z_{p1}} \right)^{-\mathbf{1}} \tag{2.21}$$

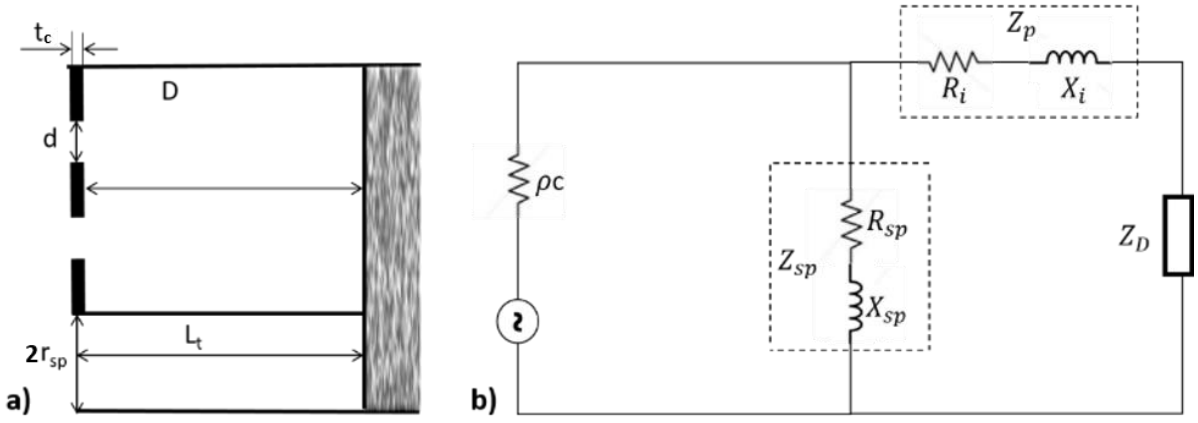

Fig. 3 - a) Parallel-arranged of an MPP and Archimedean-inspired cavity; b) Electro-Acoustical equivalent circuit parallel-arranged of an MPP and Archimedean-inspired cavity

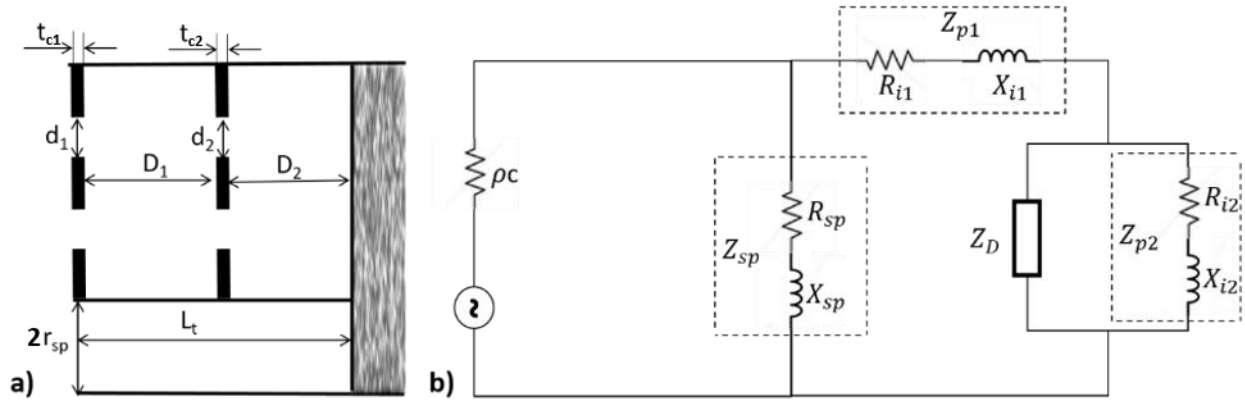

Fig. 4 - a) Parallel-arranged of double-layer MPP and Archimedean-inspired cavity; b) Electro-Acoustical equivalent circuit parallel-arranged of double-layer MPP and Archimedean-inspired cavity

3. Optimisation model

An optimisation process was preliminarily performed to model acoustic properties of the structurers, in order to design an optimised structure for broadband and high absorption in the desired frequency range. In the next paragraphs, an analytical algorithm was modelled for both MPP and AIS to study the effect of the geometrical properties on the absorption performance of the system and evaluate the optimal parameters for acoustic absorption.

3.1. Archimedean-inspired spirals

Based on Eq. (2.6), the absorption coefficient for a single cavity can be evaluated by Eq. (3.1)[28]:

$$\boldsymbol{\alpha} = \mathbf{1} - \left|\frac{(\mathbf{Z_{sp}} - \mathbf{Z_{c_0}})}{(\mathbf{Z_{sp}} + \mathbf{Z_{c_0}})}\right|^2 \tag{3.1}$$

Where the terms in absolute value is the reflection coefficient of the system. Based on Eq. (3.1), the absorption coefficient is mainly related to the acoustic impedance of the system, which is dependent on the radius r_{sp} and length of the cavity L_t. With this regard, the optimisation process is performed by evaluating the optimum radius and length based on such the value of the acoustic impedance of the system Z_{sp} that leads to full absorption (i.e. $\alpha = 1$). The optimisation is controlled by firstly studying the term $\mathrm{cotg}(kL_t)$ in Eq. (2.6) which refers to the quarter wavelength and the criterion to obtain full absorption (i.e. $\alpha = 1$).In this scenario,using Eq. (2.6), Eq. (3.1) can be rewritten as:

$$\left(\frac{\mathbf{Z_{ac}}}{\mathbf{Z_{c0}}}\right)[-\mathbf{j}\mathbf{cotg}(\mathbf{kL}_t)/\boldsymbol{\varphi}] = \frac{\mathbf{Z}_{sp}}{\mathbf{Z_{c0}}} \tag{3.2}$$

In accordance with Eqs. (3.1)-(3.2), full absorption can be achieved by matching the input impedance of the cavity matched that of the air ($Z_{sp} = Z_{c0}$). Additional multiple resonance frequencies of systems arise, which can be evaluated as follows:

$$\mathbf{Z_{c0} - Z_{ac}(-j\,cotg\,kL_t/\varphi) = 0} \tag{3.3}$$

According with Eq. (3.3), full absorption occurs at the odd harmonics of the full absorbed frequency, which represents the solution solutions of Eq (3.3) (i.e. $k = \omega/c$). Optimisation process of the main parameters of the cavities was performed according with full absorption condition in Eq. (3.2) (i.e. $Z_{sp}=Z_{c0}$).

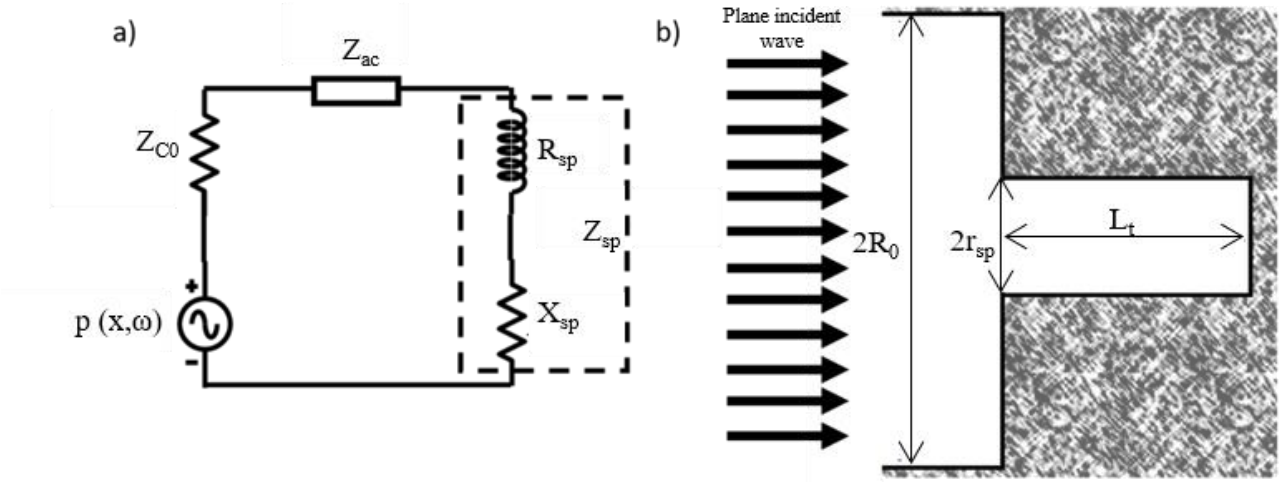

Fig. 5 a) Electro-Acoustical equivalent circuit of a cavity.; b) Wave propagation inside finite cavity.

The optimal radius of the cavity r_{sp} can be estimated by studying its relationship with the porosity of the system φ. According with Eq. (3.2) and Eq. (3.3), the value of porosity φ_{full} to obtain full absorption at a certain frequency f_0 was evaluated as follows:

$$\boldsymbol{\varphi_{full} = \frac{Z_{sp}}{Z_{c0}}(-j\,cotg\,kL_t)} \tag{3.4}$$

Where L_t was preliminarily put equal to the quarter wavelength of the absorbing frequency f_0 (i.e. $L_t = c/f_0$) and Z_{sp} was evaluated via parametric analysis, as a function of the radius. Consequently, the optimal radius r_{opt} is evaluated as follows:

$$\mathbf{r_{opt} = \sqrt{\varphi} R_0} \tag{3.5}$$

Furthermore, the optimal length of the cavity L_{opt} was calculated based on Eqs (3.3) – (3.5) as follows:

$$\mathbf{L_{opt} = \frac{1}{k} cot^{-1}\left(\frac{Z_{c0}}{Z_{sp}}\varphi_{full}\right)} \tag{3.6}$$

Archimedean-inspired spiral (AIS) principle was used to design the structure, in order to minimise its thickness. In these spirals, the distance between adjacent coils, measured radially out from the centre, is constant.

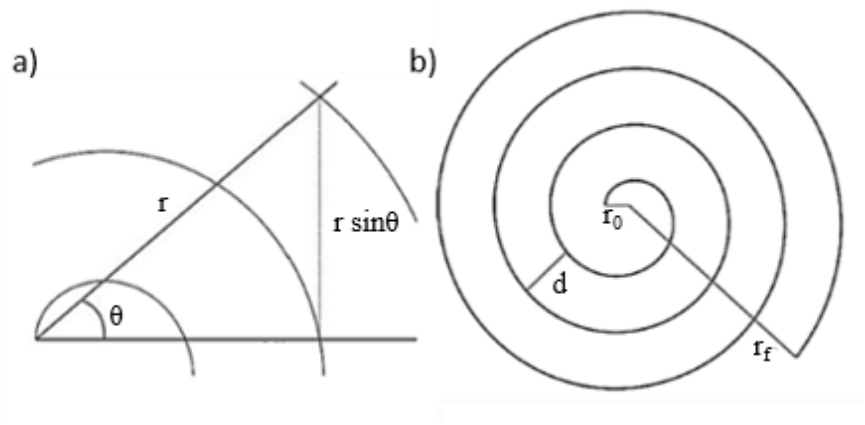

Fig. 6 - Cylindrical reference system; b) Archimedes-inspired spiral

Based on notation shown in Fig. 6, the equations in cylindrical coordinates of a spiral with initial radius r_0, final radius r_f and angle θ can be described by [33]:

$$\begin{cases} \mathbf{r = a_i + b\theta} \\ \mathbf{x = r\cos(\theta) = (a_i + b\theta)\cos(\theta)} \\ \mathbf{y = r\sin(\theta) = (a_i + b\theta)\sin(\theta)} \end{cases} \quad (3.7)$$

Where the parameter $b = (a_f - a_i)/2\pi n$ represents the growth ratio of the spiral, and n is the number of the turns of the spirals. Consequently, the length of the spiral can be estimated as follows:

$$\mathbf{L_t = \int_{a_i}^{b} \sqrt{r^2 + (dr/d\theta)^2}\, d\theta} \quad (3.8)$$

3.2. MPP Optimisation

As discussed previously, absorption performance of an MPP is strictly related to the geometrical parameters of the perforated panel. In order to evaluate the main parameters of the panel and maximise the sound absorption over a defined frequency range, an analytical model involving parametrical analyses of the geometrical factors (i.e. back cavity D, perforation ratio p, hole diameter d and thickness t_c) was developed,. Numerical integration of the absorption coefficient was applied via the trapezoidal method in order to discretise the nonlinear function α in such a way that parametric analysis of the absorption can be performed [34]. In this context, the approximation of the function α(ω) for an integration with n+1 points can be evaluated as follows[35]:

$$\int_a^b \alpha(\omega)\, d\omega = \frac{b-a}{2n}\sum_{i=1}^{n}[\alpha(\omega_i) + \alpha(\omega_{i+1})] = \frac{b-a}{2n}[\alpha(\omega_1) + 2\alpha(\omega_2) + \cdots + 2\alpha(\omega_n) + \alpha(\omega_{n+1})] \quad (3.9)$$

Where a and b represent the lower and upper limit of the interval, respectively. The discretised function was evaluated in the desired frequency interval for each combination of cavity depth D, hole diameter d, panel thickness t_c and perforation ratio p, to evaluate the values which maximise the function α in Eq. (2.21) over the desired frequency interval.

3.3. Optimisation results

Based on the optimisation analysis, three structures with different configurations and absorption frequencies were analytically studied, which are composed of two parallel-arranged MPP and Archimedean-inspired spiral with different frequency ranges (S1 and S2), and a parallel-arranged double-layer MPP and spiral (S3) . The optimal geometrical parameters evaluated for each structure are summarised in Table 1.

Table 1 - Optimal parameters for structure 1,2 and 3.

S1	**S2**	**S3**	
	MPP (2200 Hz)	**MPP** (650 Hz)	**MPP1**(950 Hz)	**MPP2** (2300 Hz)
Depth D [mm]	10.5	16	10	13
Hole Diameter d [mm]	0.5	1.2	1	0.5
Perforation ratio p [%]	3.8	14.2	2.76	0.9
Panel thickness t [mm]	1.7	0.5	1	1
----------	**AIS** (550 Hz)	**AIS** (400 Hz)	**AIS** (550 Hz)	
Length L_t [mm]	122	208	122	
Radius r_{sp} [mm]	3.48	4.14	3.48	

Total Thickness [mm]	18	24.2	28.4	

4. Analytical Results

α coefficients were evaluated according with Eq (2.19), for each structure described in table 1. In addition, the acoustic resistance and reactance of each configuration were studied to increase knowledge of the physical mechanisms involved in the absorption properties of the structures. Fig. 8 shows the α-coefficient of S1, where absorption peaks occur at the design frequency of the AIS (i.e. 550 Hz) and its 3rd and 5th harmonics (i.e. 1650 Hz and 2750 Hz), as well as at the resonance frequency of the MPP at 2200 Hz. The absorption profile is given by the superposition of each sub-system contribution included in the parallel arrangement.

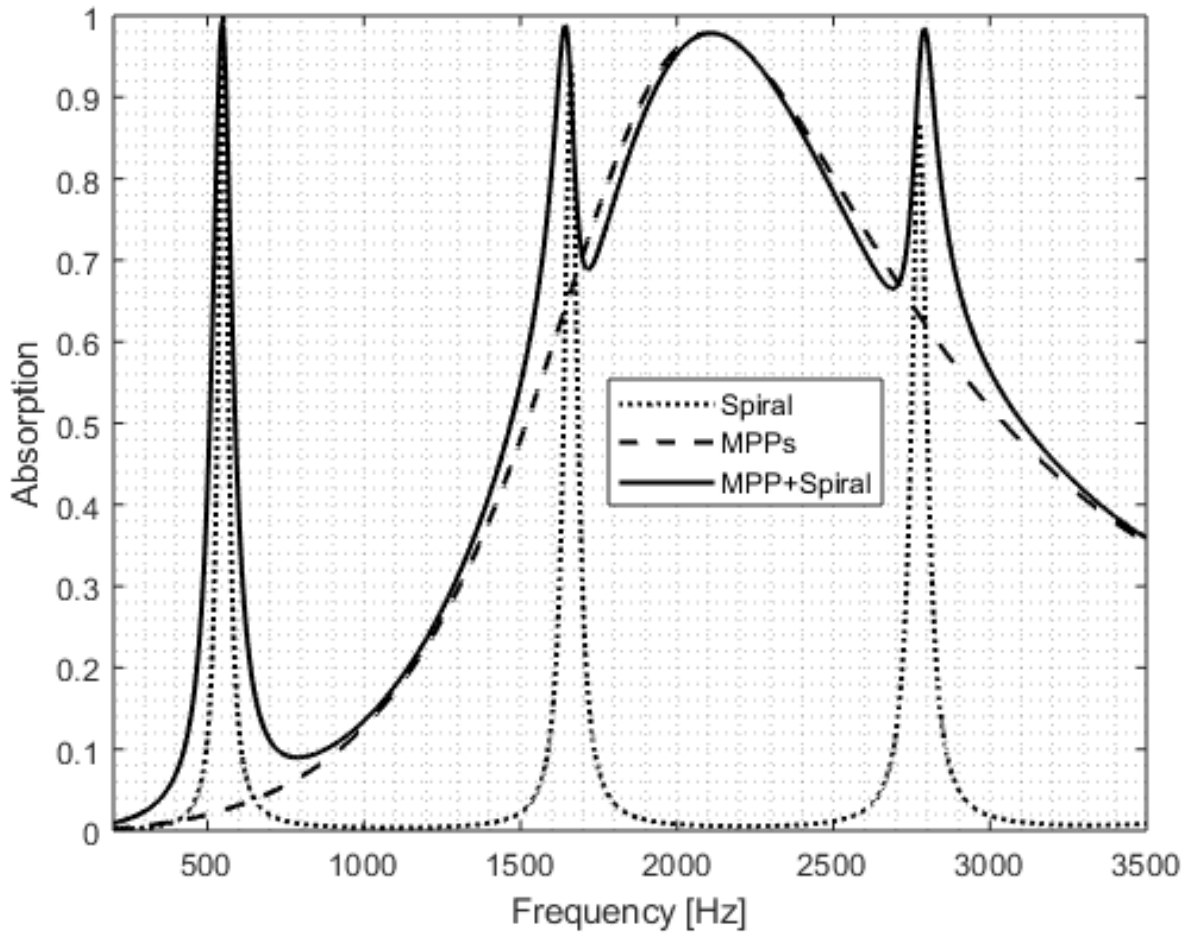

Fig. 7 - Predicted absorption coefficient for S1.

The absorption coefficient of S1 as well as that of its sub-systems are shown in Fig. 7. The real and imaginary parts of the acoustic impedance are shown in Fig. 8. Absorption peaks occur at the odd multiples of the resonance of the AIS, which also corresponds to the minima of the acoustic resistance (Fig. 8a). Moreover, minima in acoustic reactance of the system (Fig. 8b) occur at the even multiples of the resonant frequencies of the spiral (i.e. 1100 Hz, 2200 Hz and 3300 Hz), which correspond to frequency value making the term cotg(kL_t) infinite in Eq.(3.3). Acoustic resistance peaks also occurred at these frequencies. As a result, the impedance of the system is fully active, i.e. fully-constructive interference arises at that frequencies between the incident and reflected waves. In the parallel arrangement, acoustic resistance peaks are slightly right-shifted on account of the increasing trend of the resistance of the MPP added to the system.

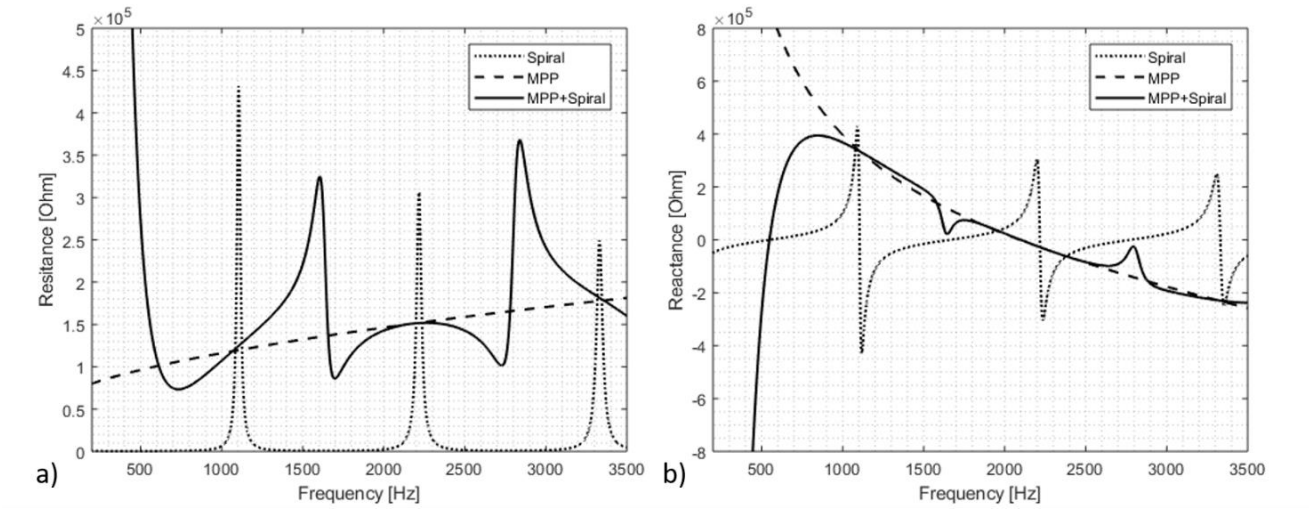

Fig. 8 - Acoustic impedance for S1. a) Acoustic resistance; b) Acoustic reactance.

Absorption coefficient for S2 is shown in Fig. 9. Absorption peaks occur at the resonant frequency of the MPP (i.e. 650 Hz) and at the multiple resonance of the AIS at 400 Hz, 1200 Hz and 2000 Hz. Fig. 11a shows acoustic resistance peaks at the anti-resonant frequencies of the structure, while inflection points of the imaginary part of the acoustic impedance (Fig. 10b) occur in correspondence of all the resonant and anti-resonant frequencies. Fig. 11 shows the absorption coefficient of S3. In this case, resonant frequencies of MPP1 and MPP2 are set between the absorption frequency f_0 and 3rd harmonic of the spiral (i.e. 550 and 1650 Hz), and the 3rd and 5th harmonics (i.e. 1650 and 2750 Hz), respectively. Acoustic resistance and acoustic reactance for structure 3 are reported in Fig. 12.

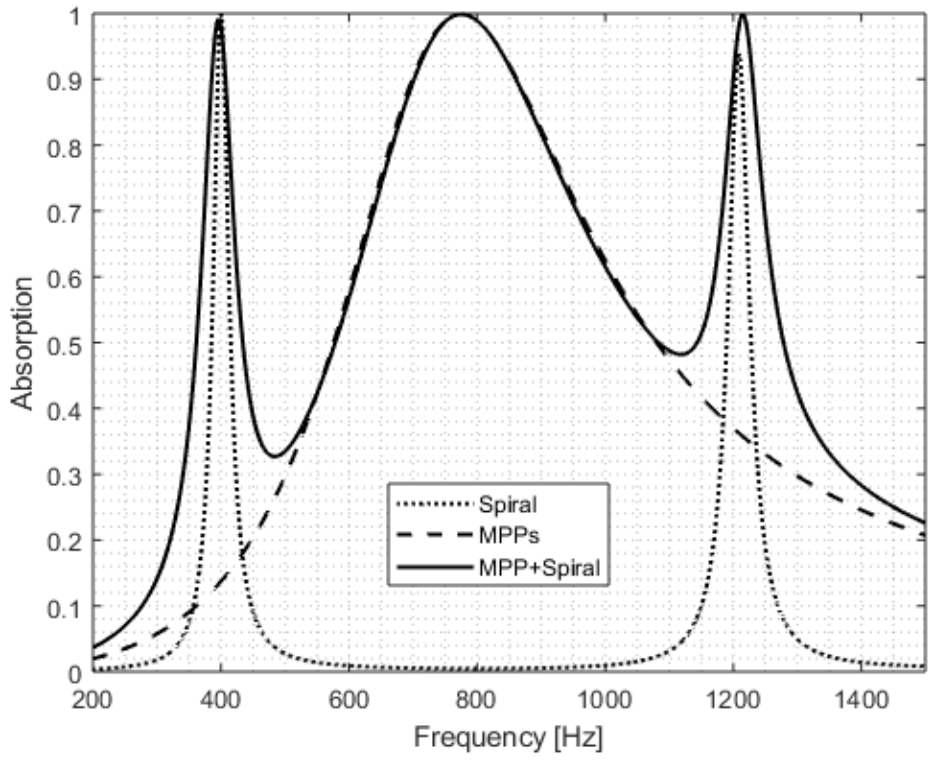

Fig. 9 - Predicted absorption coefficient for S2.

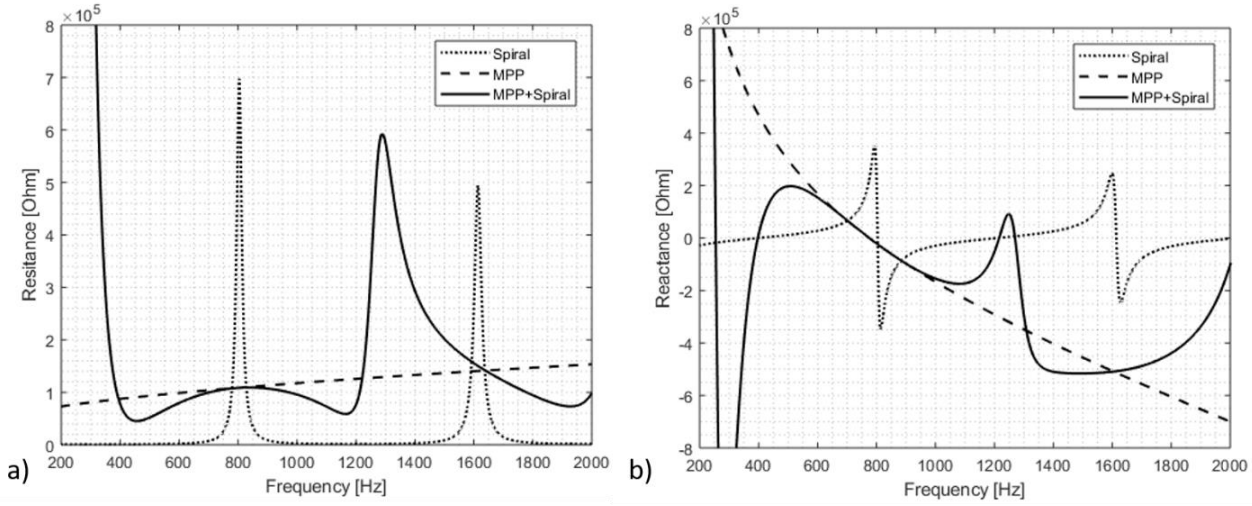

Fig. 10 - Acoustic impedance for S2. a) Acoustic resistance; b) Acoustic reactance.

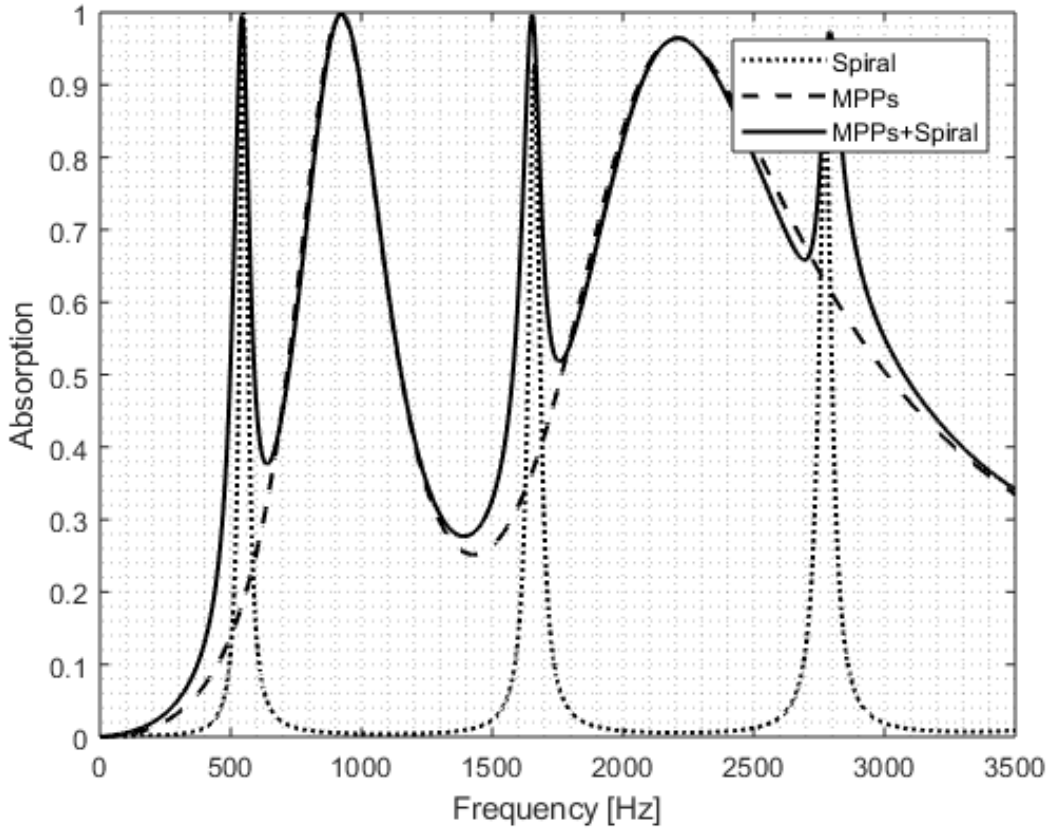

Fig. 11 - Predicted absorption coefficient for S3.

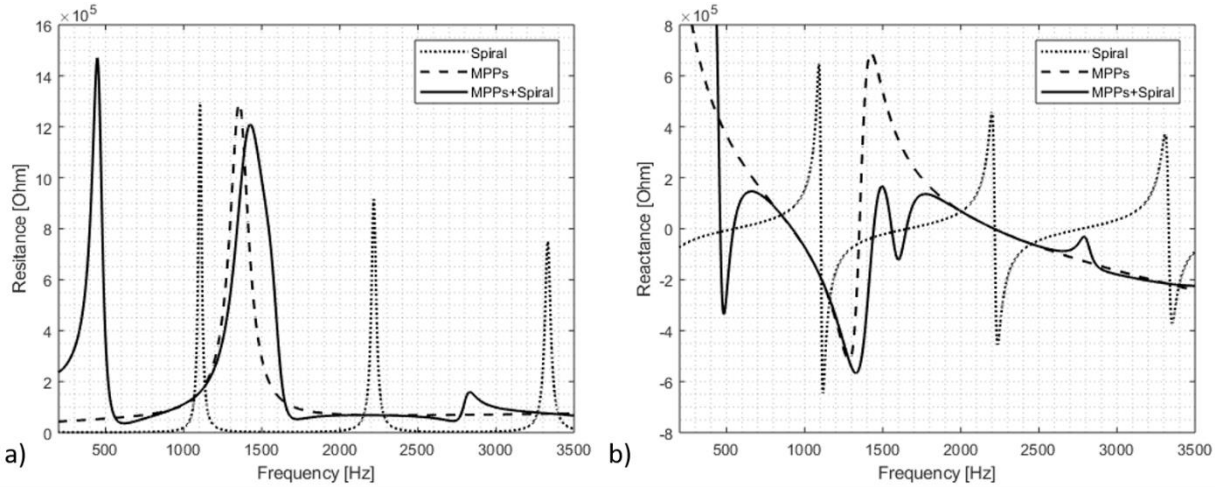

Fig. 12 - Acoustic impedance for S3. a) Acoustic resistance; b) Acoustic reactance.

5. Experimental Setup

Experimental investigations were conducted to validate the analytical models of the proposed hybrid structures. Absorption coefficient evaluation for normal plane waves were performed by means of a standard two-microphone impedance tube system. As shown in Fig. 13, the structures were placed at one end of the tube, with a broadband loudspeaker positioned at the other end. Two microphones were housed upstream from

the sample and spaced 330 mm (s_{mic}) to measure and decompose the pressure field in its incident and reflected contributions. The test rig was developed to achieve plane standing wave propagation inside the tube. The latter consisted of an aluminium tube with a thickness of 15 mm and internal diameter of 50.8 mm. The operating frequency range depends on the design of the tube. The upper frequency limit f_u depends on the diameter of the tube d_t, as follows:

$$\mathbf{f_u} < \frac{\mathbf{0.586\ c}}{\mathbf{d_t}} \tag{5.1}$$

The lower frequency limit f_l is related to the distance between the two microphones s_{mic}, which may exceed one percent of wavelength concerning the lower frequency limit, and is given by:

$$\mathbf{f_l} > \frac{\mathbf{c}}{\mathbf{100\ s_{mic}}} \tag{5.2}$$

Additionally, in order to sense propagating plane wave, microphone spacing may not exceed 80% of the half wavelength of the lower frequency limit f_l.

$$\mathbf{s_{mic}} > \frac{\mathbf{c}}{\mathbf{2.5\ f_u}} \tag{5.3}$$

The normal absorption was evaluated in accordance with the Transfer Function Methods [36]. In this context, complex reflection coefficient in Eq. (3.1) was estimated as follows:

$$\mathbf{R = R_r + jX_r = \frac{H - e^{-jks_{mic}}}{e^{jks_{mic}} - H} e^{2jk(l+s_{mic})}} \tag{5.3}$$

With H being the transfer function calculated from the complex ratio of the Fourier Transform of the sound pressures at the microphones, *l* the distance between the sample and the closer microphone. The three prototypes were then designed (Fig. 14) and fabricated by Stereolithography 3D printing technology[37].

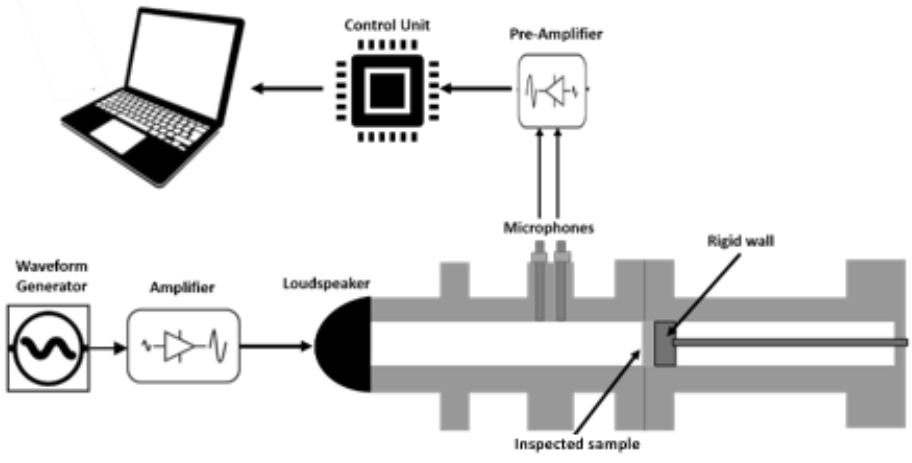

Fig. 13 - Impedance tube, Experimental Set-Up.

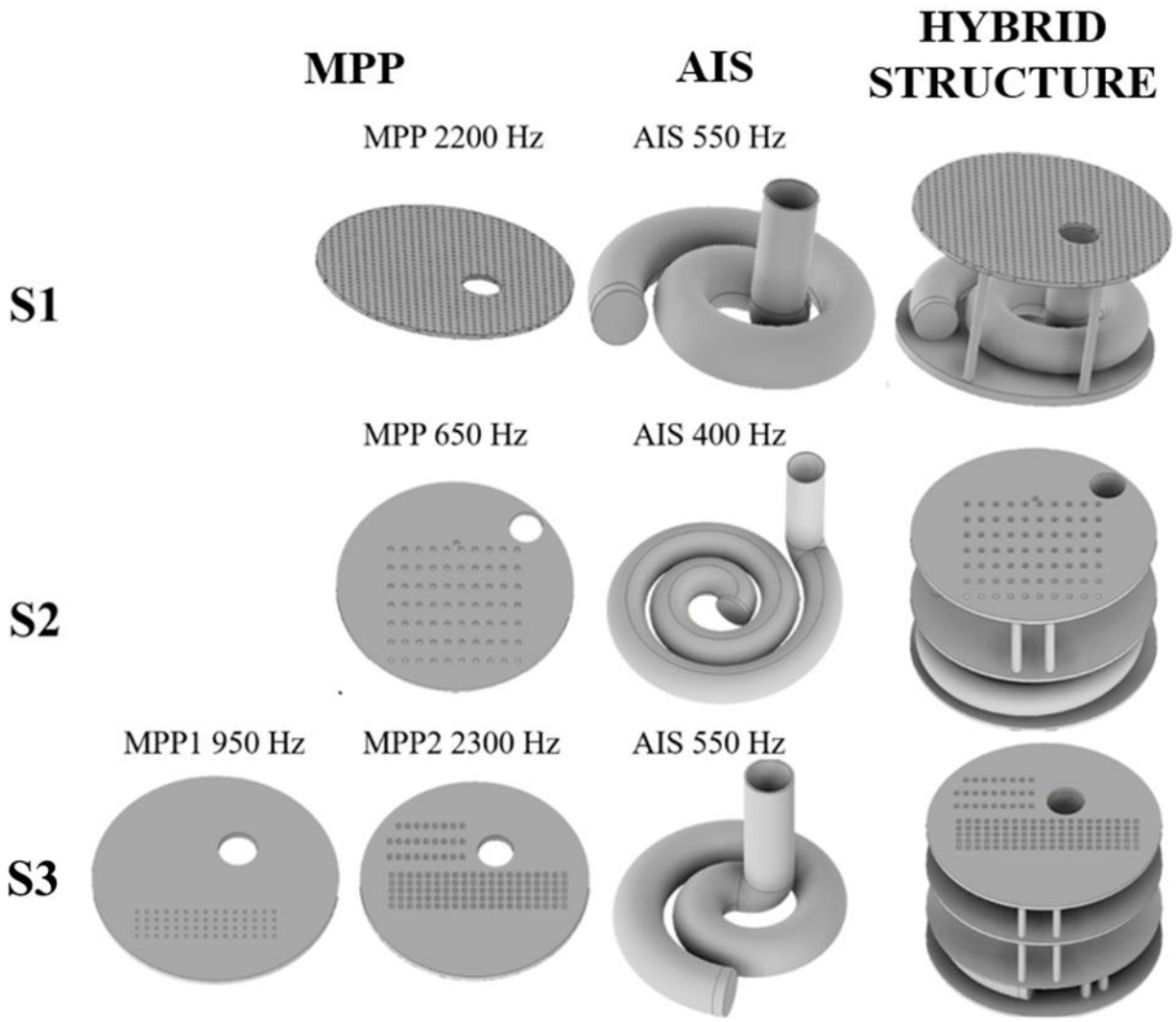

Fig. 14 – Designed MPP-AIS Hybrid Structures S1, S2 and S3.

6. Result and Discussion

Fig. 15 reports α for S1 (i.e. parallel arrangement of AIS at 550 Hz with MPP at 2200 Hz) measured according with Eq. (3.1), where absorption peaks occurred at the multiple resonances of the spiral and that of the perforated panel at 2200 Hz. Results show good correlation of the first peak at 540 Hz, while the other harmonics at 1650 and 2750 Hz are shifted to the left by 70 and 140 Hz, respectively. These effects are probably due to some additional viscous effects and mutual interferences between the two subsystems.

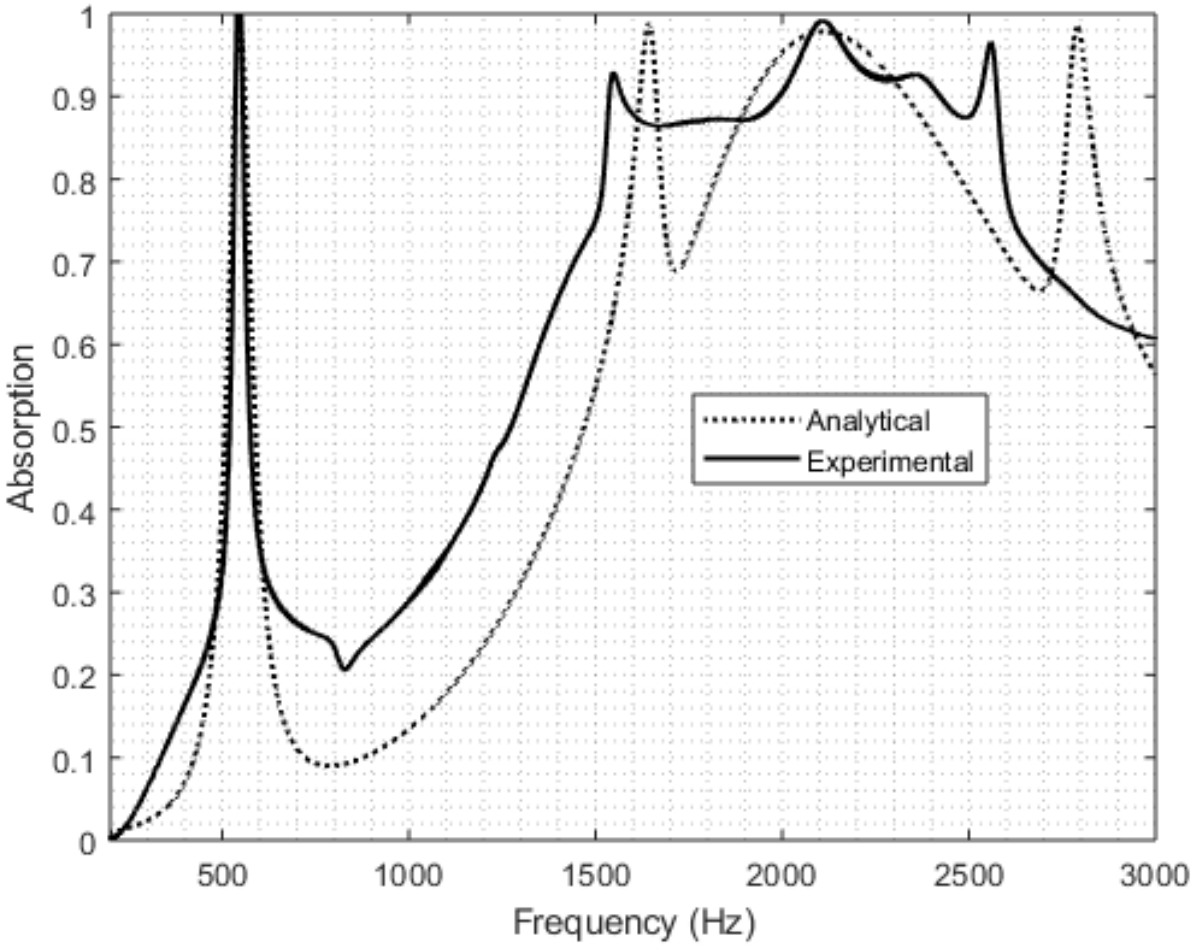

Fig. 15 - Absorption coefficient for S1 (MPP 2200 Hz, AIS 550 Hz)

Experimental results related to S2 (parallel arrangement of AIS at 400 with MPP at 650 Hz) and S3 (parallel arrangement of AIS at 550 Hz with series arrangement of MPP1 at 950 Hz and MPP2 at 2300 Hz) are shown in Figs. 16-17, respectively. In both cases, experimental results show a strong agreement with the analytical model. However, the resonances predicted by the analytical model result strongly damped compared with the measured ones. Such effect could be related to viscous losses arising with the mutual sub-system (Spiral and MPP) interaction which was not considered in the proposed analytical model. Therefore, the measured absorption profile shows wider absorption around the resonance.

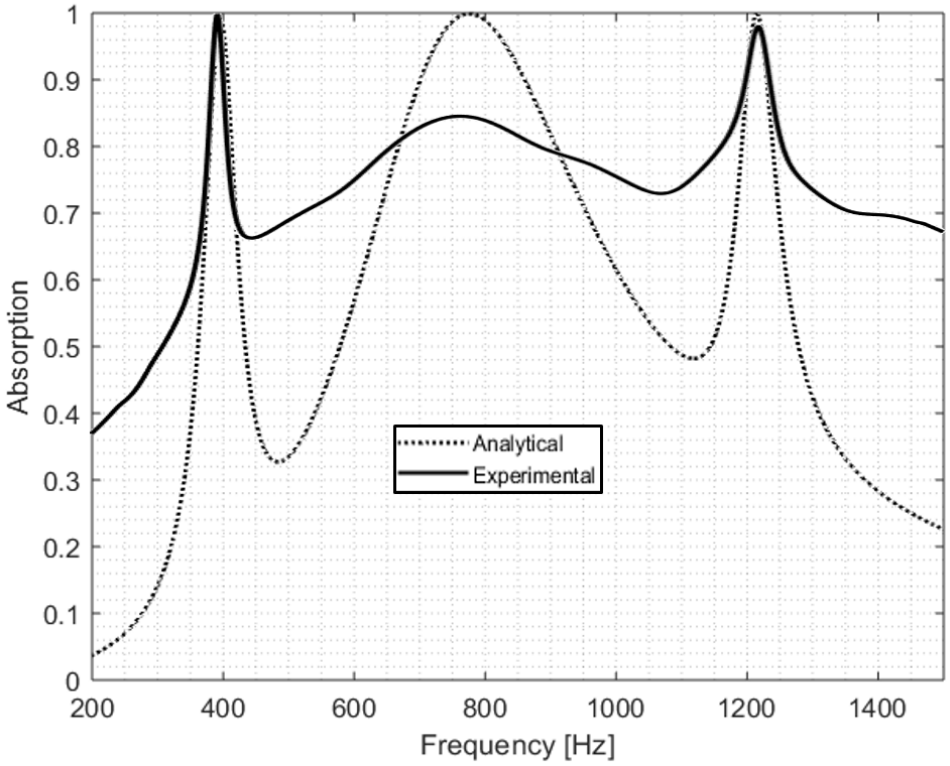

Fig. 16 – Absorption coefficient for S2 (MPP 650 Hz, AIS 400 Hz)

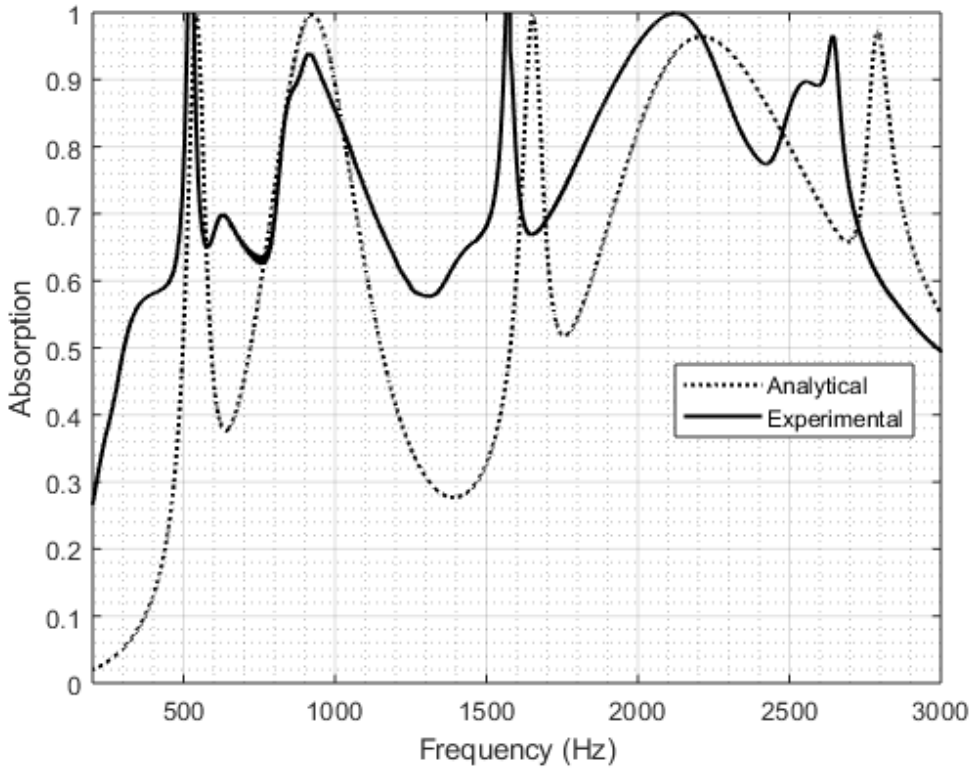

Fig. 17 – Absorption coefficient for S3 (MPP1 950 Hz, MPP2 2300 Hz and AIS 550 Hz)

7. Conclusion

In this paper, a hybrid structure consisting of a parallel-arrangement of MPP system and Archimedean-inspired spiral is proposed for application as an efficient sound absorber. An analytical algorithm was developed to model acoustic properties of the prototype and optimise the geometrical parameters of the structures for acoustic absorption. Three optimised structures were modelled with different configurations and frequency ranges, in accordance with the resonance frequencies of the MPPs and multiple resonances occurring in deep-subwavelength spiral cavity. Two parallel arrangement of MPP and AIS were designed to perform sound absorption in frequency ranges between 1550-2650 Hz and 380-1250 Hz. A parallel arrangement including an AIS and a double-layered MPP system were also designed, in order to achieve broadband absorption over 60%. Experimental results show a good correlation with the predicted model, with absorption peaks of the resonance frequencies and harmonics of the sub-systems over 90%, as well as broadband absorption along the designed frequency range for all the prototypes being proposed. Sound manipulation mechanisms achieved by the proposed hybrid MPP/AIS structures may provide a deep-subwavelength (i.e. total thickness is up to 37 times smaller than the wavelength) and insights into efficient sound absorbing design for sound filtering and noise control in real applications.

References

1. Komkin A, Mironov M, Bykov A. Sound absorption by a Helmholtz resonator. *Acoustical Physics.* 2017;63(4):385-392.
2. Kim S, Kim Y-H, Jang J-H. A theoretical model to predict the low-frequency sound absorption of a Helmholtz resonator array. *The Journal of the Acoustical Society of America.* 2006;119(4):1933-1936.
3. Wei P, Croënne C, Tak Chu S, Li J. Symmetrical and anti-symmetrical coherent perfect absorption for acoustic waves. *Applied Physics Letters.* 2014;104(12):121902.
4. Li R-Q, Zhu X-F, Liang B, Li Y, Zou X-Y, Cheng J-C. A broadband acoustic omnidirectional absorber comprising positive-index materials. *Applied Physics Letters.* 2011;99(19):193507.
5. Bucciarelli F, Meo M. Broadening sound absorption coefficient with hybrid resonances. *Applied Acoustics.* 2020;160:107136.
6. Mei J, Ma G, Yang M, Yang Z, Wen W, Sheng P. Dark acoustic metamaterials as super absorbers for low-frequency sound. *Nature communications.* 2012;3(1):1-7.
7. Sakagami K, Morimoto M, Koike W. A numerical study of double-leaf microperforated panel absorbers. *Applied acoustics.* 2006;67(7):609-619.
8. Sakagami K, Morimoto M, Yairi M. A note on the effect of vibration of a microperforated panel on its sound absorption characteristics. *Acoustical science and technology.* 2005;26(2):204-207.
9. Zwikker C, Kosten CW. *Sound absorbing materials.* Elsevier; 1949.
10. Lei L, Zuomin W, Zaixiu J. Effect of sound-absorbing material on a microperforated absorbing construction. *Chinese Journal of Acoustics.* 2011;30(2):191-202.

11. Maa D-Y. Theory and design of microperforated panel sound-absorbing constructions. *Scientia Sinica.* 1975;18(1):55-71.
12. Maa D-Y. Potential of microperforated panel absorber. *the Journal of the Acoustical Society of America.* 1998;104(5):2861-2866.
13. Maa D-Y. Microperforated-panel wideband absorbers. *Noise control engineering journal.* 1987;29(3):77-84.
14. Kang J, Brocklesby M. Feasibility of applying micro-perforated absorbers in acoustic window systems. *Applied Acoustics.* 2005;66(6):669-689.
15. Asdrubali F, Pispola G. Properties of transparent sound-absorbing panels for use in noise barriers. *The Journal of the Acoustical Society of America.* 2007;121(1):214-221.
16. Wu MQ. Micro-perforated panels for duct silencing. *Noise Control Engineering Journal.* 1997;45(2):69-77.
17. Sakagami K, Fukutani Y, Yairi M, Morimoto M. Sound absorption characteristics of a double-leaf structure with an MPP and a permeable membrane. *Applied acoustics.* 2014;76:28-34.
18. Sakagami K, Morimoto M, Yairi M. A note on the relationship between the sound absorption by microperforated panels and panel/membrane-type absorbers. *Applied Acoustics.* 2009;70(8):1131-1136.
19. Pan J, Guo J, Ayres C. Improvement of sound absorption of honeycomb panels. Paper presented at: Proceedings of ACOUSTICS2005.
20. Sakagami K, Yamashita I, Yairi M, Morimoto M. Effect of a honeycomb on the absorption characteristics of double-leaf microperforated panel (MPP) space sound absorbers. *Noise Control Engineering Journal.* 2011;59(4):363-371.
21. Wang C, Huang L. On the acoustic properties of parallel arrangement of multiple micro-perforated panel absorbers with different cavity depths. *The Journal of the Acoustical Society of America.* 2011;130(1):208-218.
22. Guo W, Min H. A compound micro-perforated panel sound absorber with partitioned cavities of different depths. *Energy Procedia.* 2015;78:1617-1622.
23. Bucciarelli F, Fierro GM, Meo M. A multilayer microperforated panel prototype for broadband sound absorption at low frequencies. *Applied Acoustics.* 2019;146:134-144.
24. Jacobs PF. *Rapid prototyping & manufacturing: fundamentals of stereolithography.* Society of Manufacturing Engineers; 1992.
25. Voet VS, Strating T, Schnelting GH, et al. Biobased acrylate photocurable resin formulation for stereolithography 3D printing. *ACS omega.* 2018;3(2):1403-1408.
26. Allard J, Atalla N. *Propagation of sound in porous media: modelling sound absorbing materials 2e.* John Wiley & Sons; 2009.
27. Kang J, Fuchs H. Predicting the absorption of open weave textiles and micro-perforated membranes backed by an air space. *Journal of sound and vibration.* 1999;220(5):905-920.
28. Chen C, Du Z, Hu G, Yang J. A low-frequency sound absorbing material with subwavelength thickness. *Applied Physics Letters.* 2017;110(22):221903.
29. Johnson DL, Koplik J, Dashen R. Theory of dynamic permeability and tortuosity in fluid-saturated porous media. *Journal of fluid mechanics.* 1987;176:379-402.
30. Cai X, Guo Q, Hu G, Yang J. Ultrathin low-frequency sound absorbing panels based on coplanar spiral tubes or coplanar Helmholtz resonators. *Applied Physics Letters.* 2014;105(12):121901.
31. Morse PM, America ASo, Physics AIo. *Vibration and sound.* Vol 2: McGraw-Hill New York; 1948.
32. Crandall IB. *Theory of vibrating systems and sound.* D. Van Nostrand Company; 1926.
33. Carvalho De Sousa A, Deckers E, Claeys C, Desmet W. PARALLEL ASSEMBLY OF ACOUSTIC RESONATORS TO OBTAIN NARROW-BAND UNITY SOUND ABSORPTION PEAKS BELOW 1000 HZ. *http://www icedyn net/.* 2019.
34. Kythe PK, Schäferkotter MR. *Handbook of computational methods for integration.* CRC Press; 2004.
35. Golubitsky M, Dellnitz M. *Linear algebra and differential equations using MATLAB.* Brooks/Cole Publishing Co.; 1999.
36. Chung J, Blaser D. Transfer function method of measuring in-duct acoustic properties. I. Theory. *The Journal of the Acoustical Society of America.* 1980;68(3):907-913.

37. Griffey J. 3-D printers. *Library technology reports.* 2014;50(5):23-30.